

## Vehicle-induced aerodynamic loads on highway sound barriers part1: field experiment

Dalei Wang, Benjin Wang\* and Airong Chen

*Department of Bridge Engineering, Tongji University, Shanghai, 200092, China*

*(Received February 27, 2013, Revised June 7, 2013, Accepted July 11, 2013)*

**Abstract.** The vehicle-induced aerodynamic loads bring vibrations to some of the highway sound barriers, for they are designed in consideration of natural wind loads only. A field experiment is carried out with respect to three important factors: vehicle type, vehicle speed and the vehicle-barrier separation distance. Based on the results, the time-history of pressures is given, showing identical characteristics in all cases. Therefore, the vehicle-induced aerodynamic loads acting on the highway sound barrier are summarized as the combination of “head impact” and “wake impact”. The head impact appears to have potential features, while the wake impact is influenced by the rotational flow. Then parameters in the experiment are analyzed, showing that the head impact varies with vehicle speed, vehicle-barrier separation distance, vehicle shape and cross-sectional area, while the wake impact is mainly about vehicle-barrier separation distance and vehicle length.

**Keywords:** vehicle-induced aerodynamic loads; highway sound barriers; field experiment

---

### 1. Introduction

Since the traffic noise has drawn increasing attention and concern nowadays, sound barriers were set up on highways as an important means to reduce the noise. However, some of them were found to suffer from premature fatigue failure, see Fig. 1. The vibrations on highway sound barriers were observed while vehicles are passing by, which might be responsible for the fatigue failure. The current design specifications, such as Chinese design code for wind resistance (JTG/T D60-01-2004), only consider natural wind loads, leave the vehicle-induced aerodynamic loads ignored. The UK standard for determination of loading on temporary road signs was also “generally perceived by the industry to be unrealistic, in that no account is taken of vehicle induced forces” (Quinn *et al.* 2001b).

The study of vehicle-induced aerodynamic loads was originated from the aerodynamic loads induced by trains. Due to the high speed of the trains, many works were done in studying the aerodynamics of trains passing by each other (Fujii and Ogawa 1995), the train moving into tunnels (Ogawa and Fujii 1996, Shin and Park 2003) or stations (Gerhardt and Krüger 1998). Baker (2008) described the flow field around high speed trains and revealed the nature of it. Besides, the European Standard (EN 14067-4: 2005, Section 5) defines the train-induced pressure

---

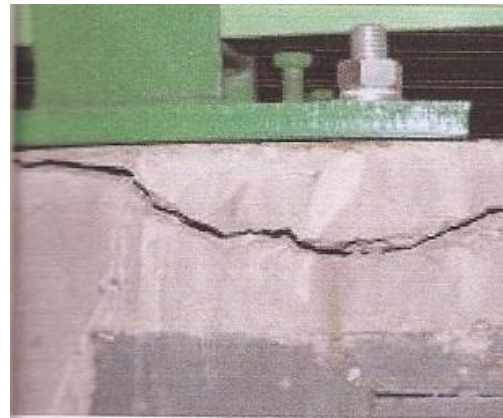
\*Corresponding author, PhD student, E-mail: [wbj8259168@126.com](mailto:wbj8259168@126.com)

changes causing loading on flat vertical structures parallel to the tracks. However, it is not applicable for determining the vehicle-induced aerodynamic loads, since the vehicle types and travel paths are more complicated on highways.

Similarly, the high speed of road vehicles also encouraged the study of aerodynamic loads induced by vehicles. The effects of vehicle-induced aerodynamic loads were firstly studied by Cali and Covert (2000). By measuring the loads on a model of overhead highway sign, it was observed that the most severe wind load occurred on sign panel that is positioned perpendicular to the vehicle motion at the moment that the front of the vehicles were passing by. The force was mainly dependent on both the vehicle speed and the area of the sign. By conducting field experiments, Quinn *et al.* (2001b) checked Cali and Covert's conclusions, and addressed that the vehicle nose shape, the elevation of sign were also important factors in this issue. In addition, their tests on perpendicular and parallel pedestrian barriers indicated that the different orientation would lead to different patterns of vehicle-induced aerodynamic loads. Sanz-Andrés *et al.* (2002, 2003, 2004) provided the theoretical supports in vehicle-induced aerodynamic load on signs and pedestrian barriers under the assumption of potential flow.



(a) Sound barrier deformation



(b) Concrete cracking at root of sound barrier

Fig. 1 Effects on highway sound barriers by vehicle-induced aerodynamic load

Thus, the previous studies covered the vehicle-induced aerodynamic loads on signs and pedestrian barriers. As for the highway sound barrier, its parallel orientation and larger scale creates a different boundary condition of the flow field, which may lead to different characteristics of load sensitivity. Researches on the free-standing walls were helpful in studying the load on sound barriers, for the similar boundary conditions they produce. Works made by Letchford and Holmes (1994), Robertson *et al.* (1995, 1996, 1997), Letchford and Robertson (1999) and Holmes (2001) focused on the natural wind load by wind tunnel tests and full-scale tests, yet the effect of vehicle-induced aerodynamic load was not included.

Works reported here are focused on the vehicle-induced aerodynamic load on highway sound barriers. By performing field experiment, the time-history curves of vehicle-induced aerodynamic load on highway sound barriers are obtained. With respect to three variables (vehicle type, vehicle

speed, vehicle-barrier separation distance), the results collected by the field experiment are analyzed and discussed.



(a) Volkswagen Passat (VP)



(b) Toyota Coaster (TC)



(c) Kinglong Coach XMQ6118MMC (KC)

Fig. 2 Experimental vehicles

## 2. Field experiment

The field experiment location was on the eastern part of Ningbo Circle Highway, near the famous scenic area of Dongqian Lake. Due to the close location to the residential area and high design speed (120 km/h), it is inevitable to set up sound barriers to avoid traffic noise problem. The erection of sound barrier was in progress then, therefore provided the conditions for the experiment.

### 2.1 Basic scheme

Due to the transient nature of the flow induced by passing vehicles, it was necessary to concentrate on the instantaneous value rather than the time average one. Therefore the experiment

was designed to measure the pressure on the sound barrier only for a short period of time. The data were collected by differential pressure transducers when certain kinds of vehicles were passing by the experimental sound barrier with different speeds and vehicle-barrier separation distances.

Referring to the previous studies, the following three important variables were taken into account in this experiment: vehicle type, vehicle speed and vehicle-barrier separation distance.

## 2.2 Variables

### 2.2.1 Vehicle type

Concerning the main parameters such as vehicle shape and scale, three typical vehicle types were determined to be Kinglong Coach XMQ6118MMC (KC), Toyota Coaster (TC) and Volkswagen Passat (VP). VP is a representative of cars with small size and streamlined shape, while TC & KC are representatives of coaches with moderate/large size and box shape, see Fig. 2. The main parameters of these vehicle types are shown in Table 1.

Table 1 Parameters of typical vehicle types

Vehicle type	KC	TC	VP
Vehicle shape	Box	Box	Streamlined
Vehicle scale (length×width×height) (mm)	11480×2490×3460	6990×2025×2585	4789×1765×1470



Fig. 3 Distance marks on the road

### 2.2.2 Vehicle speed

The vehicle speed should be as fast as possible to get good measurements. Given the conditions of the experiment site, vehicles would accelerate for about 200 meters, and then try to keep the speed constant while it was close to the experimental sound barrier. However, it was difficult to stabilize the speed, as the dashboard readings were changing during the process. Thus, the vehicle speed was recorded by a portable GPS device, GARMIN 200 W. The device can measure the

vehicle speed and update every second, which means the speed is the average value per second. In this short period of time, the effect of speed fluctuation can be ignored, and the vehicle speeds were considered constant.

### 2.2.3 Vehicle-barrier separation distance

The vehicle-barrier separation distance was controlled by experiment participants who drive the above mentioned kinds of vehicles with their left wheels running over the distance marks. As shown in Fig. 3, these marks were painted on the road in experimental preparation. The horizontal distance to the hard shoulder were 3.7 m, 3.2 m and 2.7 m, and numbered as 1#~3#, respectively. By subtracting the vehicle width from it, the minimum separation distance can be obtained.

### 2.3 Data collection

Each piece of sound barrier consisted of three acoustic absorption bodies and one acrylic transparent panel inserting in the gap between two H-shaped steel columns. However, as Fig. 4 shows, the experimental one replaced the transparent panel with another two acoustic absorption bodies to go through the pressure tube.

Measuring points were uniformly set in a distribution of 5 rows and 3 columns, i.e., 15 in total.

For each measuring point, there were two tubes connecting to a differential pressure transducer, one on the positive pressure port, and the other on the reference pressure port. The latter one sensed the pressures on the back side of sound barrier, while the former one, with its tube going through the barrier body to the front, obtained the pressures on the road side. The transducer, Setra Model 264, would sense this pressure difference and convert to a proportional analog output voltage. To reduce the equipment error, the tubes were 5 mm in I.D. and no longer than 0.5 m in length. Considering the extra shape, instruments were all installed on the back side of the sound barrier.



Fig. 4 Measuring points arrangements and instruments connection

As mentioned before, every vehicle events seemed to behave transiently and lasted about 3 seconds. And the measured pressures at the corresponding time of vehicles passing were much bigger than the background ones, so the vehicle-induced aerodynamic pressure could be easily distinguished.

Table 2 Performance specifications of differential pressure transducer Setra Model 264

Name	Range	Accuracy	Nonlinearity	Hysteresis	Non-repeatability	Weight
Setra Model 264	0 ~ ±50in.W.C.	±1.0%FS	±0.96%FS	0.2%FS	0.05%FS	285 grams

## 2.4 Experimental cases

A total of seventeen cases were completed, with varying vehicle type, vehicle speed and vehicle-barrier separation distance, see Table 3.

Table 3 Summary of experimental cases

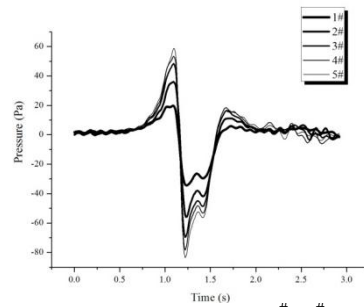
Vehicle type	Case name	Vehicle speed (km/h)	Distance Mark	Minimum Distance (m)
Kinglong Coach	KC-1	72	2#	0.96
	KC-2	90	2#	0.96
	KC-3	87	1#	1.46
	KC-4	82	1#	1.46
	KC-5	77	2#	0.96
Toyota Coaster	TC-1	80	3#	0.925
	TC-2	85	2#	1.425
	TC-3	87	3#	0.925
	TC-4	72	3#	0.925
	TC-5	77	2#	1.425
	TC-6	76	3#	0.925
	TC-7	80	2#	1.425
Volkswagen Passat	VP-1	122	2#	1.685
	VP-2	103	1#	2.185
	VP-3	113	2#	1.685
	VP-4	115	3#	1.185
	VP-5	110	2#	1.685

## 3. Results and discussions

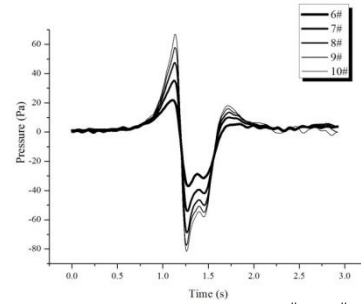
### 3.1 Time-history of pressures

Take case TC-1 for instance, Fig. 5 shows the pressure difference induced by vehicles on measuring points of the same rows/columns. Obviously, the results on the same column reach the positive/negative peak simultaneously, but with different values. In contrast, the ones in the same

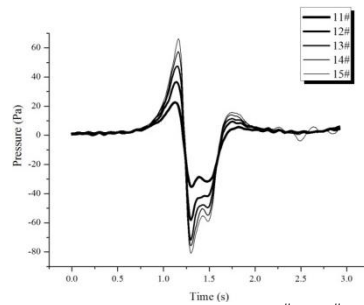
row get similar values with interval time. Besides, it appears to have some disturbance on the positive peak of measuring points 1#~5#, which is probably caused by the nearby H-shaped steel column. In consideration of the spatial and column effects, the result of measuring point 10# are presented and analyzed hereinafter, since it is able to represent the responses on other points.



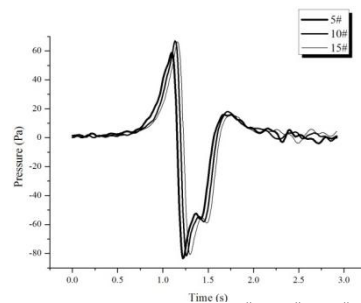
(a) the first column (1#~5#)



(b) the second column (6#~10#)



(c) the third column (11#~15#)



(d) the lowest row (5#, 10#, 15#)

Fig. 5 Experimental results on measuring points of the same rows/columns in case TC-1

According to the results of all cases, the time-history of vehicle-induced aerodynamic loads on sound barrier can be summarized as follows: as vehicle moves closer, the pressure increases and reaches the positive peak, then sharply jumps to a negative one in a very short period of time. Then a second pressure jump with opposite direction and smaller amplitudes follows closely. So the pressure jump occurs twice in a vehicle event. In consideration of the relative position of vehicle and sound barrier, the first one is called “head impact”, and the second one is called “wake impact”.

The profile of head impact is consistent with the one Sanz-Andrés *et al.* (2004) derived by potential flow theory. Therefore it is assumed to be a consequence of potential flow. However, the apparent larger negative amplitudes in VP cases imply that the head impact and wake impact overlap each other on certain conditions. Therefore, the case of KC-2 is taken to give a clearer definition of head/wake impact, as Fig. 6 shows.

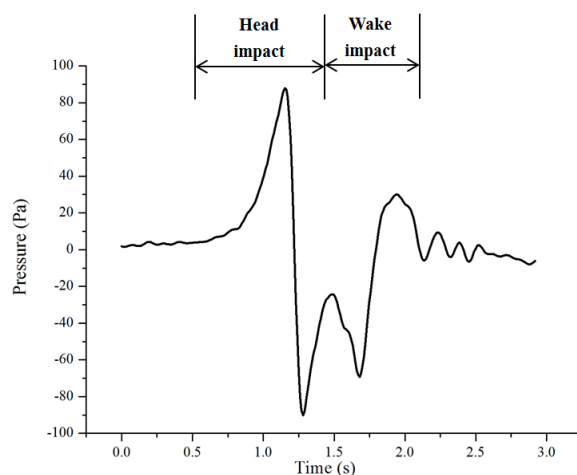


Fig. 6 Definition of head impact and wake impact (e.g., KC-2, measuring point 10#)

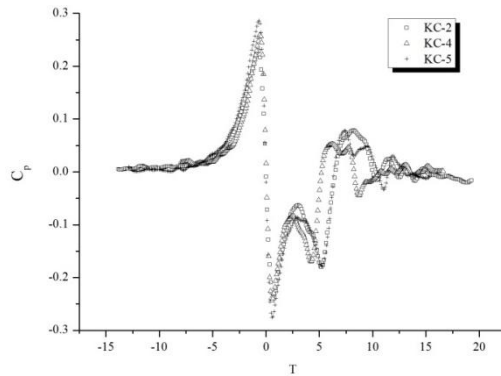
By selecting typical values of variables, the pressure time-history curves of eight cases are presented in Fig. 7. It differs from the experimental results (Fig. 8 in Quinn *et al.* 2001b) of pedestrian barriers in that the sound barrier is more prone to the wake impact. The experimental results are shown in dimensionless forms by introducing  $C_p$  (for the pressure) and  $T$  (for time) defined as follows

$$C_p = \frac{\Delta p}{\frac{1}{2} \rho v^2} \quad (1)$$

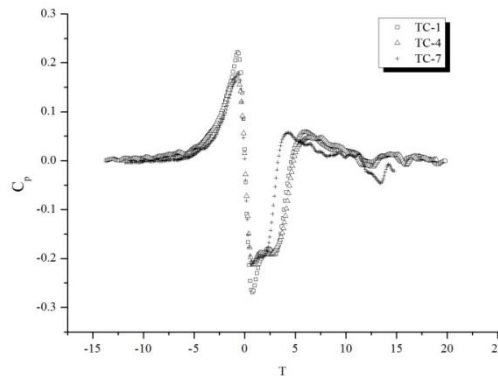
where  $\Delta p$  is the pressure,  $\rho$  is the density of air,  $v$  is vehicle speed.

$$T = \frac{(t - t_0)v}{d_c} \quad (2)$$

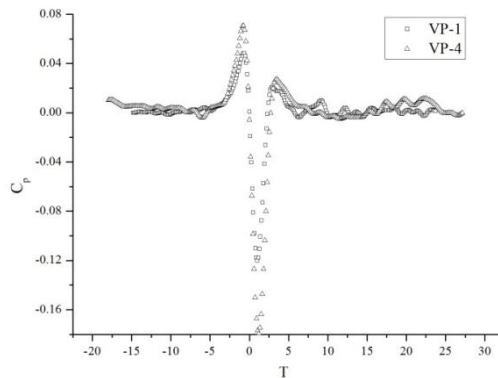
where  $d_c = d_m + \frac{1}{2}W_v$ ,  $d_m$ , is the minimum separation distance,  $W_v$  is the width of the vehicle,  $t_0$  is the reference time, which is define as the zero-crossing time from first positive peak to negative peak.



(a) Typical KC cases



(b) Typical TC cases



(c) Typical VP cases

Fig. 7 Experimental results on measuring point 10<sup>#</sup>

### 3.2 Discussion on variables

#### 3.2.1 Vehicle speed

Works of Sanz-Andrés *et al.* (2002, 2003, 2004) have already proved that the square of vehicle speed is proportional to the wind load, as shown in Eq. (3), where  $v_1, v_2$  are the vehicle speed in different cases and  $\Delta p_{1max}, \Delta p_{2max}$  are the maximum value of pressure, respectively

$$\left(\frac{v_1}{v_2}\right)^2 = \frac{\Delta p_{1max}}{\Delta p_{2max}} \tag{3}$$

In the case of KC-1, 2, 5 & TC-1, 3, 4, 6 & VP-1, 3, 5, the effect of vehicle speed would be illustrated, because of the same vehicle-barrier separation distance there. Fig. 8 gives the linear fit for max/min pressure to square of vehicle speed, shows that the expectation is acceptable, though with some errors, which will be discussed in the following sections.

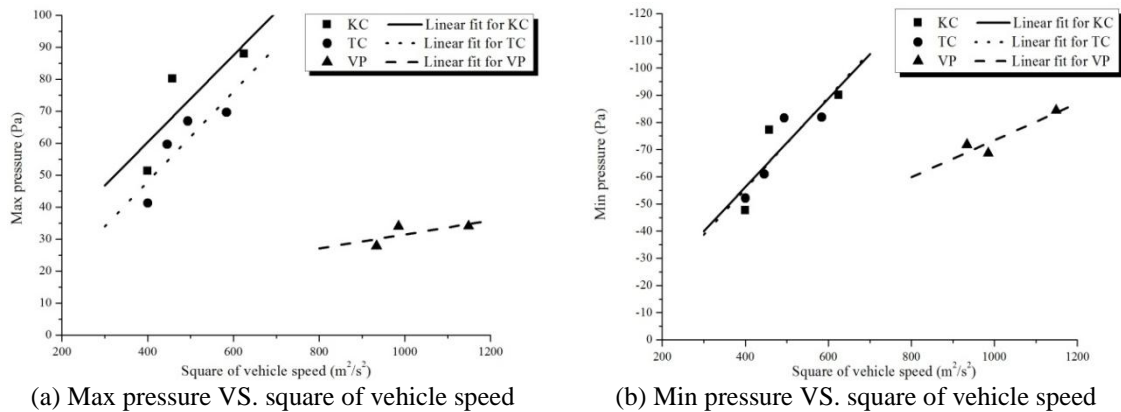


Fig. 8 Variation of max/min pressure with square of vehicle speed

#### 3.2.2 Vehicle-barrier separation distance

For the large scale of sound barrier, the vehicle-barrier separation distance should be divided into two parts: the horizontal one determined by the distance mark and the vertical one determined by the height of measuring point. However, by integrating the pressures on measuring points, the force on the whole sound barrier can be achieved, so that the effects of vertical part are avoided.

Similar to the vehicle-sign analysis proposed by Quinn *et al.* (2001b), a dimensionless coefficient  $C_F$  is introduced, which is defined as Eq. (4)

$$F = \frac{1}{2} C_F \rho v^2 A \tag{4}$$

where  $F$  is the force on sound barrier,  $\rho$  is the density of air,  $v$  is vehicle speed,  $A$  is the cross-sectional area.

$C_F$  is a function of horizontal vehicle-barrier separation distance, vehicle length and vehicle

shape. The latter two factors are interferences in discussing the effects of horizontal separation distance. Fig. 9 shows the variation of  $C_{Fmax}$  and  $C_{Fmin}$  with  $d_c$ , and their inverse square curve fit. Sum of Squared Error (SSE) is introduced to reveal the performance of fit. The smaller SSE for  $C_{Fmax}$  indicates that it nearly fits an inverse square curve, which proves the potential feature of head impact, whereas the larger one for  $C_{Fmin}$  means that the corresponding suction force is influenced by the overlapping wake impact.

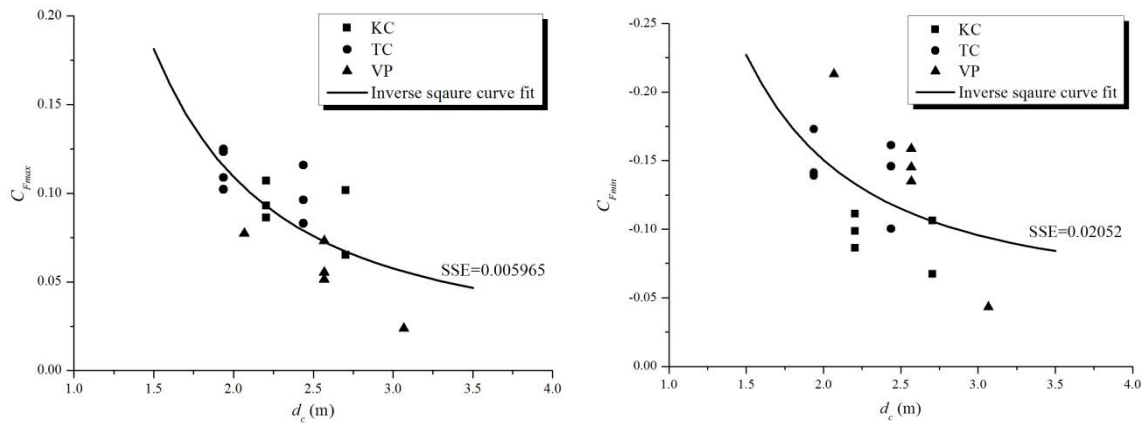


Fig. 9 Variation of  $C_{Fmax}$  and  $C_{Fmin}$  with  $d_c$

### 3.2.3 Vehicle type

There are considerable differences between vehicle types, which can be analyzed in three aspects: vehicle shape, vehicle length and cross-sectional area. Addressed in previous studies (Cali and Covert 2000, Sanz-Andrés *et al.* 2002, 2003, 2004), the larger cross-sectional area undoubtedly leads to higher pressure peaks. That explains the greater amplitudes in KC cases even with lower speeds.

Another difference is the interval from head impact to wake impact. As they are overlapping each other in VP cases, the two negative peaks occur almost simultaneously, leading to the disproportionate high negative peaks. Since the head impact occurs close to the vehicle head, it is helpful to define the interval time between the first positive peak and the second negative peak to indicate the location that the wake impact occurs. A reduced interval time is introduced to describe the effect of vehicle length, which is defined as Eq. (5)

$$R_t = vt_1 / L \tag{5}$$

Where  $t_1$  is the interval time between the first positive peak and the second negative peak,  $L$  is the vehicle length.

Fig. 10 gives the variation of reduced interval time with vehicle type. As  $R_t$  is approximately around the value of one in almost all cases, it implies that the vehicle end is near the location where the most intense wake impact occurs.

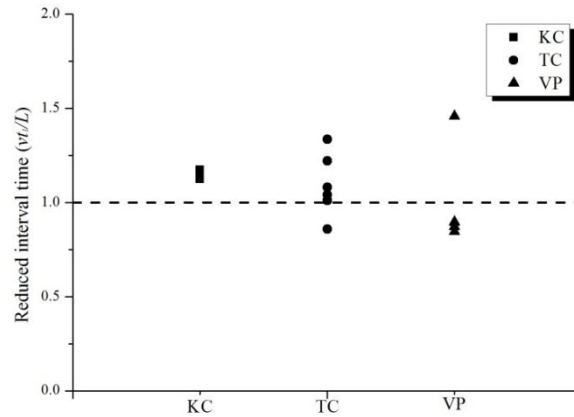


Fig. 10 Variation of reduced interval time with vehicle type

As for the vehicle shape, it is difficult to quantify the magnitude for its actions to pressure peaks. To establish the relations between vehicle shape and pressure, one dimensionless coefficient  $C_s$  is introduced as it excludes other variables, which is defined as Eq. (6)

$$C_s = \frac{\Delta p d_c^2}{\frac{1}{2} \rho v^2 A} \quad (6)$$

Fig. 11 gives the  $C_{Smax}$  and  $C_{Smin}$  for each vehicle type, and Table 4 shows the mean values. The KC and TC cases reach approximate values of  $C_{Smax}$  for the same box shape they have, while the smallest  $C_{Smax}$  in VP cases indicates that the streamlined shape certainly reduces the positive peak. On the other hand, the largest  $C_{Smin}$  in VP cases shows the streamlined shape leads to largest negative peaks. Besides,  $C_{Smin}$  in TC cases are larger than that in KC cases, which might be another proof that the vehicle length affects the negative peak.

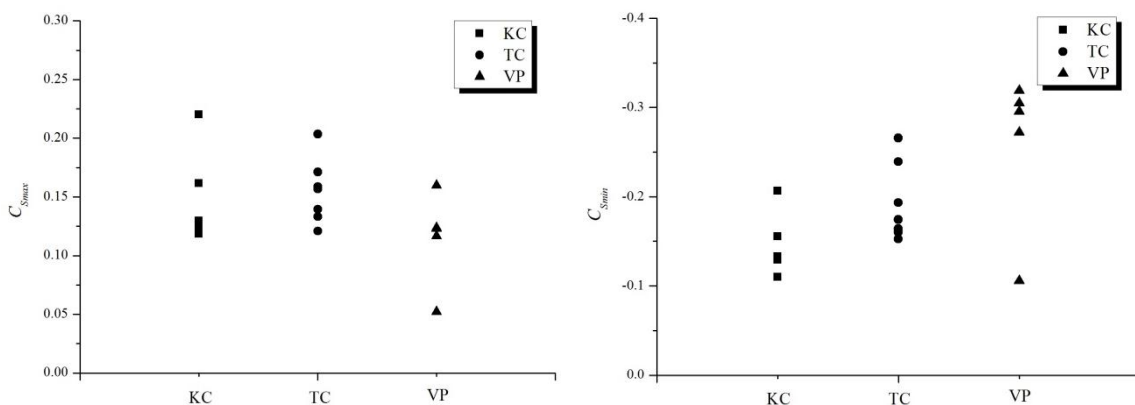


Fig. 11 Comparison of  $C_{Smax}$  and  $C_{Smin}$  of different vehicle types

Table 4 Mean value of  $C_{Smax}$  and  $C_{Smin}$  of different vehicle types

Vehicle type	KC	TC	VP
Mean value of $C_{Smax}$	0.1508	0.1548	0.1151
Mean value of $C_{Smin}$	-0.1467	-0.1928	-0.2594

### 3.3 Error analysis

First of all, it is necessary to mention that in the case of VP-2, the small size and large separation (>2 m) distance could only produce a relatively low pressure. Thus some errors may be introduced by the background responses. That is the reason for the discrete point of VP cases in Figs. 10 and 11.

Other errors that occurred in the experimental results may be the consequences of two aspects: system error and personal error. The system error could be neglected as the experimental details explained. The personal error in this experiment is the main part, and it comes from the inaccuracy in determining the vehicle-barrier separation distance. Due to the concern of risks, it is difficult for the drivers to keep the distance close enough to meet the plan exactly. Besides, drivers' adjustment to meet the requiring distance mark might lead to strong disturbance of air flow, which may highly affect the wake of vehicle. However, the statistic characteristics in all cases still appear to be in agreement to reach conclusions.

## 4. Conclusions

In the field experiment, the vehicle-induced aerodynamic loads on highway sound barriers were collected with respect to three variables: vehicle type, vehicle speed and vehicle-barrier separation distance, and then the results were analyzed and discussed. The main conclusions are summarized as follows.

The vehicle-induced aerodynamic load goes from a positive peak to a negative one in a short period of time, followed by a second pressure jump with opposite direction and smaller amplitudes. Although its magnitude is always lower than that of natural wind loads specified in design code, the vehicle-induced aerodynamic loads has to be taken into account in design phase, for it causes alternating stress on structures which could lead to fatigue problems.

The whole time-history of vehicle-induced aerodynamic load can be divided into two main parts: "head impact" and "wake impact". Based on the experimental results, the head impact appears to have potential features and the wake impact is related to the rotational flow. Furthermore, the wake impact sometimes overlaps the head impact, leads to a high negative peak.

Then the effect of each variable is analyzed separately. Firstly, the square of vehicle speed is proportionate to the maximum and minimum pressure, as the widely perceived conclusion indicates.

The effects of vehicle-barrier separation distance are more complicated than that in the vehicle-sign problem, for the non-negligible scale the sound barriers have. The results show its relation with the maximum pressure is nearly inverse quadratic.

The effect of vehicle type differs from not only the vehicle scale but also the vehicle shape. The former one consists of two parts: cross-sectional area and vehicle length. The cross-sectional area

is well studied before and perceived to have effect on the head impact, while the vehicle length may have influence on the wake impact. The vehicle shape is hard to give a definition with quantitative values, for there are too many parameters to be taken into account. It is better to establish a dimensionless coefficient for each type of vehicle, such as  $C_S$  in this paper. Further investigation with more types and cases is still needed.

## Acknowledgements

The work described in this paper was financially supported by National Natural Science Foundation of China, Grant No. 51008234. The authors also would like to express the thanks to Highway Management Bureau of Ningbo and Shanghai Zhongchi Construction and Engineering Ltd., for their supports and assistances during the experiments.

## References

- Baker, C.J. (2001), "Flow and dispersion in ground vehicle wakes", *J. Fluid Struct.*, **15**(7), 1031-1060.
- Baker, C. (2010), "The flow around high speed trains", *J. Wind Eng. Ind. Aerod.*, **98**(6-7), 277-298.
- Barrero-Gil, A. and Sanz-Andrés, A. (2009), "Aeroelastic effects in a traffic sign panel induced by a passing vehicle", *J. Wind Eng. Ind. Aerod.*, **97**(5-6), 298-303.
- British Standards Institution (2005), *EN 14067-4, Railway Applications-Aerodynamics-Part 4: Requirements and Test Procedures for Aerodynamics on Open Track*, London, UK.
- Cali, P.M. and Covert, E.E. (2000), "Experimental measurements of the loads induced on an overhead highway sign structure by vehicle-induced gusts", *J. Wind Eng. Ind. Aerod.*, **84**(1), 87-100.
- Corin, R.J., He, L. and Dominy, R.G. (2008), "A CFD investigation into the transient aerodynamic forces on overtaking road vehicle models", *J. Wind Eng. Ind. Aerod.*, **96**(8-9), 1390-1411.
- Fujii, K. and Ogawa, T. (1995), "Aerodynamics of high speed trains passing by each other", *Comput. Fluids.*, **24**(8), 897-908.
- Gerhardt, H.J. and Krüger, O. (1998), "Wind and train driven air movements in train stations", *J. Wind Eng. Ind. Aerod.*, **74-76**, 589-597.
- Hemida, H. and Baker, C. (2010), "Large-eddy simulation of the flow around a freight wagon subjected to a crosswind", *Comput. Fluids.*, **39**(10), 1944-1956.
- Holmes, J.D. (2001), "Wind loading of parallel free-standing walls on bridges, cliffs, embankments and ridges", *J. Wind Eng. Ind. Aerod.*, **89**(14-15), 1397-1407.
- Ministry of Communications of PRC. (2004), *JTG/T D60-01-2004, Specifications on Wind Resistance Design of Highway Bridges*, Beijing, China.
- Ogawa, T. and Fujii, K. (1997), "Numerical investigation of three-dimensional compressible flows induced by a train moving into a tunnel", *Comput. Fluids.*, **26**(6), 565-585.
- Quinn, A.D., Baker, C.J. and Wright, N.G. (2001a), "Wind and vehicle induced forces on flat plates-Part 1: wind induced force", *J. Wind Eng. Ind. Aerod.*, **89**(9), 817-829.
- Quinn, A.D., Baker, C.J. and Wright, N.G. (2001b), "Wind and vehicle induced forces on flat plates-Part 2: vehicle induced force", *J. Wind Eng. Ind. Aerod.*, **89**(9), 831-847.
- Sanz-Andrés, A., Laverón, A., Baker, C. and Quinn, A. (2004), "Vehicle induced loads on pedestrian barriers", *J. Wind Eng. Ind. Aerod.*, **92**(5), 413-426.
- Sanz-Andrés, A. and Santiago-Prowald, J. (2002), "Train-induced pressure on pedestrians", *J. Wind Eng. Ind. Aerod.*, **90**(8), 1007-1015.
- Sanz-Andrés, A., Santiago-Prowald, J., Baker, C. and Quinn, A. (2003), "Vehicle-induced loads on traffic sign panels", *J. Wind Eng. Ind. Aerod.*, **91**(7), 925-942.

- Shin, C. and Park, W. (2003), "Numerical study of flow characteristics of the high speed train entering into a tunnel", *Mech. Res. Commun.*, **30**(4), 287-296.
- Waymel, F., Monnoyer, F. and William-Louis, M.J.P. (2006), "Numerical simulation of the unsteady three-dimensional flow in confined domains crossed by moving bodies", *Comput. Fluids.*, **35**(5), 525-543.

CC